Broad band nonlinear optical absorption measurements of the laser dye IR26 using white light continuum Z-scan

Soumyodeep Dey, Sudhakara Reddy Bongu, and Prem Ballabh Bisht

Citation: Journal of Applied Physics **121**, 113107 (2017); doi: 10.1063/1.4978762
View online: http://dx.doi.org/10.1063/1.4978762
View Table of Contents: http://aip.scitation.org/toc/jap/121/11
Published by the American Institute of Physics

Broad band nonlinear optical absorption measurements of the laser dye IR26 using white light continuum Z-scan

Soumyodeep Dey, Sudhakara Reddy Bongu, and Prem Ballabh Bisht[a)]
Department of Physics, Indian Institute of Technology, Madras, Chennai 600036, India

(Received 2 October 2016; accepted 6 March 2017; published online 20 March 2017)

We study the nonlinear optical response of a standard dye IR26 using the Z-scan technique, but with the white light continuum. The continuum source of wavelength from 450 nm to 1650 nm has been generated from the photonic crystal fiber on pumping with 772 nm of Ti:Sapphire oscillator. The use of broadband incident pulse enables us to probe saturable absorption (SA) and reverse saturable absorption (RSA) over the large spectral range with a single Z-scan measurement. The system shows SA in the resonant region while it turns to RSA in the non-resonant regions. The low saturation intensity of the dye can be explained based on the simultaneous excitation from ground states to various higher energy levels with the help of composite energy level diagram. The cumulative effects of excited state absorption and thermal induced nonlinear optical effects are responsible for the observed RSA. *Published by AIP Publishing*. [http://dx.doi.org/10.1063/1.4978762]

I. INTRODUCTION

Organic materials are consistently withstanding their role in photonics due to their low saturation intensity, large absorption, and emission cross sections.[1] The delocalization of π-electrons over the molecular chains is the key feature resulting in high nonlinear optical (NLO) effect in these systems.[2] Heptamethine cyanine or near infrared (IR) dyes are important chromophores for photonic applications spanned into various interdisciplinary fields. Some of their applications are photodynamic therapy,[3] dye-sensitized solar cell applications,[4] fluorescence imaging,[5] near IR lasing,[6] optical limiting at telecommunication wavelengths,[7] and passive modelocking.[8] The dye IR 26 is still used in commercial lasers for generating ultrashort pulses.[9] Kalanoor and Bisht have reported the wavelength dependent NLO response of IR 26 under ps excitation.[10] Ali *et al*. have observed the modelocking capability of zinc oxide sandwiched gold nanoparticles thin films combined with low IR 26 dye concentration.[11]

The NLO response of nanomaterials such as graphene is independent of wavelength.[12,13] On the other hand, several other materials including wrapped graphene sheets,[14] metal nanoparticles, organic materials,[15] and semiconductor quantum dots have been reported to show the wavelength-dependent response. The NLO response of a system mainly depends upon the excitation wavelength, input irradiance, pulse-width, and repetition rate of the laser.[16–18] In the powerful, yet simple, Z-scan technique, the sample is moved in and out of focus to vary the incident intensity without varying the source energy. By measuring the transmitted intensity, this method enabled the researchers to study nonlinear absorption in the material and clearly identify the saturable absorption (SA) or reverse saturable absorption (RSA) threshold at the pump wavelength. The Z-scan studies are traditionally carried out with single wavelength input and will have to be repeated for every wavelength of interest. Some reports are available in the literature on broad-band nonlinear optical responses of various materials by white light continuum (WLC) Z-scan.[13,19–23]

The supercontinuum (SC) consists of wavelengths of wide spectral range with high spatial coherence. The first spectral broadening in crystals and glasses was observed by Alfano and Shapiro in 1970 with the help of high power picosecond pulses.[24] Later on, the investigations of SC generation have been done in a wide range of nonlinear materials, including solids,[25] organic and inorganic liquids,[26,27] gases,[28] and optical waveguides.[29] Photonic crystal fiber (PCF), a new class of optical waveguide, made possible to generate the SC by injecting a kW peak power optical pulses.[29] In recent years, PCF filled with different media have been found to show several advantages than the air filled PCF.[30,31] We have used continuum white light in our Z-scan measurements. This method offers a couple of advantages—enables us to obtain the nonlinear parameters for *all* wavelengths in the visible band with single Z-scan measurements and the simultaneous excitations by photons of various wavelengths reduces the threshold for SA studies at any wavelength in the band.

II. EXPERIMENTAL

A. Characterization of fundamental mode-locked pulse

Figure 1(a) shows the spectral profile of mode-locked pulses obtained from the Ti: Sapphire oscillator. The spectrum spanned from 750 nm to 790 nm with central wavelength at 772 nm. The full width at half maximum of the mode-locked pulse is ~8.3 nm. The temporal width of the mode-locked pulse was measured by using a dispersion free intensity autocorrelator.[32] Labview program and photomultiplier tube (IP 28) were used for data collection. Figure 1(b) gives the autocorrelation trace (symbols) and solid line corresponding to the Gaussian fit to the data. The estimated actual pulse width (τ_p) is ~90 fs.

[a)]E-mail: bisht@iitm.ac.in

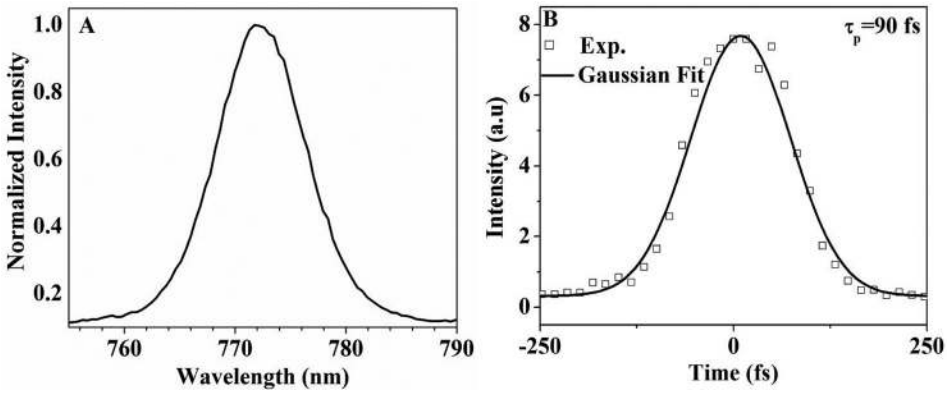

FIG. 1. Spectral (panel A) and temporal (Panel B) profiles of mode-locked pulse. τ_p is the pulse width of the laser.

B. Supercontinuum generation

The experimental setup for fs SC generation is given in Figure 2. A fs Ti-sapphire (Ti^{+3}:Al_2O_3) oscillator (TISSA100, CDP) at 772 nm centre wavelength with a repetition rate of 82 MHz and 500 mW average power was used as a pump source. It was pumped with the second harmonic of CW diode pumped neodymium yttrium vanadate (Nd:YVO_4) laser (Millennia Pro s-series). The combination of a half wave plate and a thin film Brewster type polarizer (Eksma Optics, 990-0071) was used for attenuation of the input beam. A PCF (model SCG-800, New Port) was used to generate the WLC. The objective lens (40×) was used for focusing the pump beam on to the crystal fibre, and another lens (20×) was used to collimate the WLC. The complete spectral profile of WLC was recorded by using a fiber optic spectrometer (Ocean Optics, HR2000, linear silicon CCD array) for 400 nm–1100 nm wavelength ranges and IR spectrometer (IrSys, TQ-Systems GmbH, Si and InGaAs detectors) for 600 nm–1700 nm wavelength range. The optical resolution of HR2000 spectrometer is 0.065 nm, while for IR spectrometer it is 1 nm. The average output power of the fs white light was ∼62 mW.

C. White light Z-scan experiment

The broad band nonlinear optical response of IR26 was measured by the open aperture Z-scan technique (Figure 2). The WLC was used for exciting the sample after passing through a chopper operating at 1 kHz. The chopper was used for reducing the thermal effects in the sample. The samples were taken in a 1 mm standard glass cell and scanned in the focal plane of a lens of focal length 50 mm. The transmitted light from the sample was collected by a large aperture lens of focal length 200 mm at the far field and was detected by a spectrometer (Ocean Optics, HR2000). The spectra were recorded in steps of 0.5 mm of the scan over the focal plane of the lens (L_1). The white-light spectrum with solvent alone was considered as the reference. The ratio of signal to reference spectrum gives the transmittance of the samples.

III. THEORETICAL ASPECTS

For Gaussian input beam and under the low irradiance limit, the variation in the intensity ($I(\lambda)$) of the excited beam within the nonlinear medium can be written as[33]

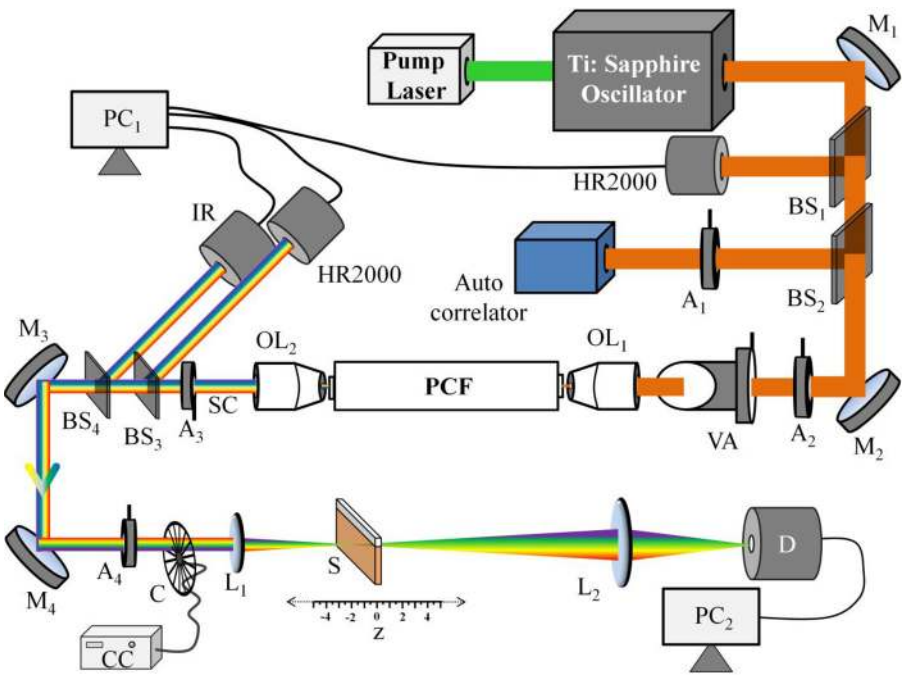

FIG. 2. Experimental layout for generation of fs SC and WL Z-scan. M_{1-4}, are the plane mirrors, BS_{1-4} are the beam splitters, A_{1-4}, are the apertures, VA is the input beam intensity attenuator, PCF is the photonic crystal fiber and OL_{1-2} are the objective lenses, SC is the supercontinuum, HR2000 is the UV-Vis spectrometer and IR is IR spectrometer. C is the chopper, CC is the chopper controller, L_{1-2} are the double convex lenses, S is the sample, D is the signal detector, and PC_{1-2} are the personal computers.

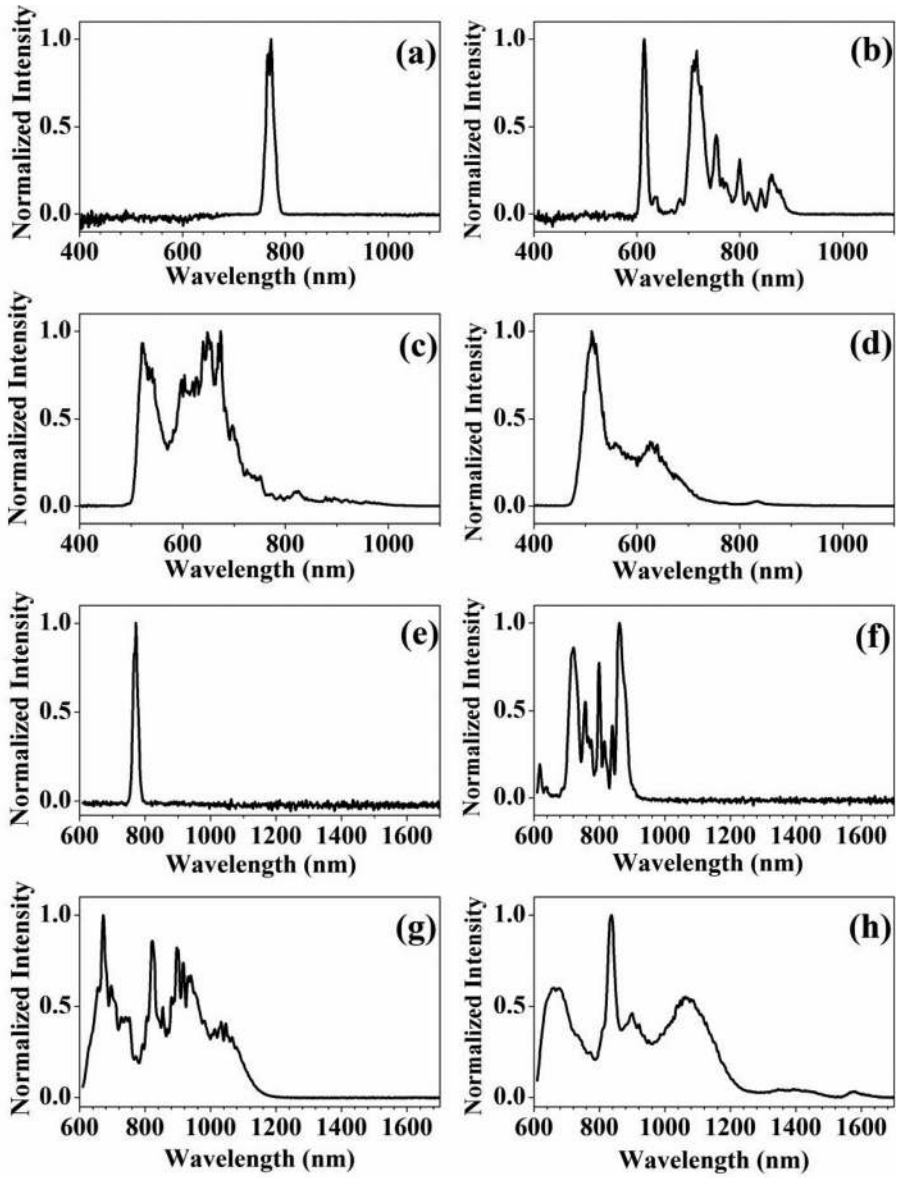

FIG. 3. Femtosecond SC spectra (normalised to unity) from PCF at various values of input power [(a) <10 mW, (b) 30 mW, (c) 170 mW, and (d) 266 mW] recorded with HR2000 spectrometer. The spectra (e) <10 mW, (f) 30 mW, (g) 170 mW, and (h) 266 mW are recorded with IR spectrometer.

$$\frac{dI(\lambda)}{dz'} = -\alpha_0(\lambda)I(\lambda) - \beta(\lambda)I^2(\lambda), \tag{1}$$

where $\alpha_0(\lambda)$ and $\beta(\lambda)$ are the linear and nonlinear absorption coefficients at the excitation wavelength (λ), respectively. z′ is the distance measured along the optical axis from the sample entrance plane. For the open aperture Z-scan case, the normalized transmittance is given by[34]

$$T(z,\lambda) = \frac{\ln(1+q_0(z,0,\lambda))}{q_0(z,0,\lambda)}, \tag{2}$$

where $q_0(z,0,\lambda) = \beta(\lambda)I_0(\lambda)L_{eff}(\lambda)/(1+x^2)$ with $L_{\text{eff}}(\lambda)$ is the effective path length at wavelength λ and x (z/z_0) is the sample travelling distance (z) normalized to the Rayleigh range (z_0). For the simultaneous occurrence of SA and RSA effects, the total intensity dependent nonlinear absorption coefficient $\alpha(I)$ is given by[34]

$$\alpha(I) = \frac{\alpha_0}{1+\left(\frac{I}{I_s}\right)} + \beta_{Eff}I. \tag{3}$$

The first term on the right-hand side corresponds to the SA contribution while the second term to the RSA. Here, β_{Eff} is the effective NLO coefficient with contributions from electronic absorption and thermal effects. The $\alpha(I)$ is related to the β in Equation (2) by $\beta = \frac{\alpha(I)-\alpha_0}{I}$. All the terms in the Equation (3) depend on the wavelength λ.

TABLE I. Generated SC power and spectral range as function of input pump power.

Coupled power (mW)	Generated SC power (mW)	Effective spectral Range (nm)
<10	…	746–795
10	…	723–820
30	4	600–926
70	12	555–1015
110	24	497–1110
170	36	483–1262
230	48	454–1646
266	57	455–1665
322	62	450–1673

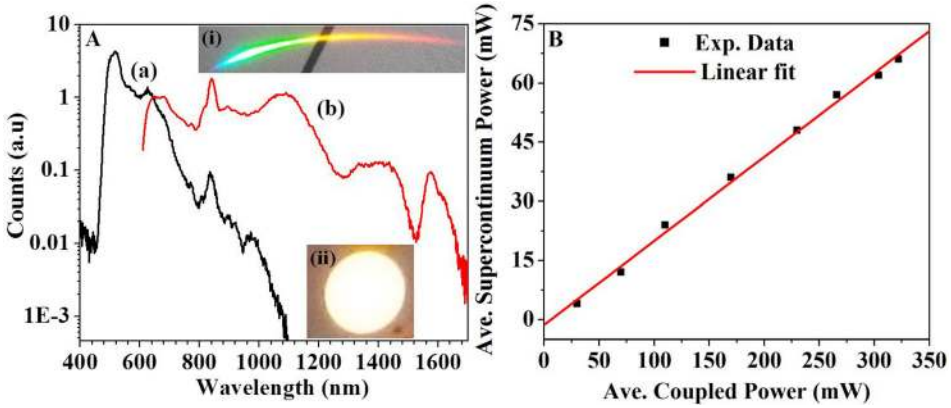

FIG. 4. Full SC spectrum (with y-scale in log) generated from PCF recorded by HR2000 spectrometer (curve (a)) and IR spectrometer (curve (b)). The spectra have been normalized at 663 nm. The inset (bottom) shows the photo of the white light spot and the inset (top) is dispersed photo of the spot with the help of a grating. Panel (b) gives the obtained average SC power with respect to the input power of fundamental beam. Symbols are experimental data and solid line is linear fit.

IV. RESULTS

A. fs supercontinuum

SC is a nonlinear optical phenomenon, in which a high intensity ultra short laser pulse spectrally broadens over several octaves on interacting with a nonlinear medium. Several individuals or cumulative nonlinear optical processes, such as self phase modulation, stimulated Raman scattering, and four-photon parametric mixing are responsible for the observation of this phenomena.[35] The mechanism for SC generation mainly varies with the pulse width of the pump laser.[36,37]

SC from PCF at various input powers recorded with the two spectrometers is shown in Figure 3. Table I gives the summary of the SC. The SC spectra from (a) → (d) and (e → h) correspond to the lower to higher input coupling powers recorded with HR200 and IR spectrometers, respectively. These spectra indicate a wide spectral range from 450 nm to 1673 nm. However, both spectra contain non-uniform intensity distribution throughout. The measured average power of the SC at this condition is 62 mW corresponding to the input coupled powers of 322 mW. From these figures, it is observed that the output of the PCF contains very weak residual of the fundamental wavelength. The WLC has been used without further any filtration for Z-scan measurements.

The full spectra generated from the PCF recorded with both the spectrometers are given in Figure 4(a). It can be seen that under the experimental conditions, the SC range of ∼450 to 1673 nm can be easily obtained. The inset-(i) of panel A shows the photo of the visible spectral contents of SC by dispersing it with the help of a grating. Bottom inset-(ii) shows the corresponding white light spot. Panel B indicates the net obtained average SC power with respect to the input coupled power. A linear fit indicates that the generated SC power is apparently proportional to the input

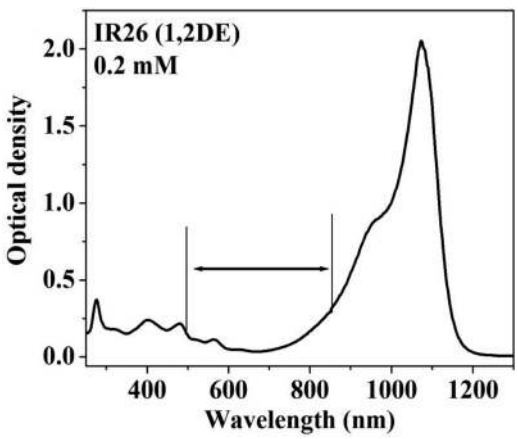

FIG. 5. Steady state absorption spectrum of IR 26 in 1,2-Dichloroethane. The range between arrows indicates the portion of wavelengths used for WL Z-scan.

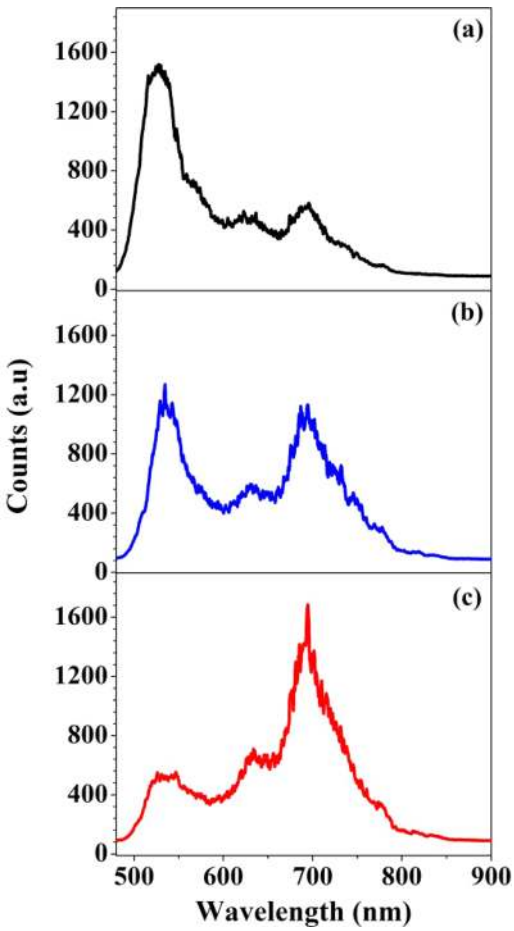

FIG. 6. Transmission spectra of IR26 at various sample position on the focal plane of lens L_1. The curves (a) and (b) are for 12 mm and 2 mm away from the focus, respectively, while curve (c) corresponding to the sample position at the focus.

power up to about 300 mW. Nevertheless, it is to be noted that with an increase in the pump power, the spectrum broadens (see Fig. 3) and the detector response has to be taken into account.

B. Broad band nonlinear optical response of dye

Figure 5 shows the steady state absorption spectrum of dye IR 26 in 1, 2-Dichloroethane. The dye shows the maximum absorption (peak at 1072 nm) in the near IR region. The entire spectrum spans from 260 nm to 1200 nm with lower absorption in the visible region.

The white light transmission spectra for IR26 at near focus and far away (a—1 mm and b—12 mm) from the focal points are shown in Figure 6. It can be seen that the spectra differ distinctly at these positions. Especially at the focus, it changes dramatically. It indicates the nonlinear absorption behaviour of the sample. The OA Z-scan profiles of IR26 were obtained at various wavelengths of excitations (Figure 7) by reconstructing the variation in the signal spectrum. Symbols are the experimental data, and solid lines are the guiding line to the eye. The profiles are exhibiting the saturable absorption (SA), reverse saturable absorption (RSA), and the combination of SA and RSA behaviour.

The SA effect was observed above 630 nm, while RSA occurs below 530 nm. The combined effects have been observed between 530 nm and 630 nm. The contributions of SA and RSA effects depend on the intensity of excitation wavelength of WLC and absorption spectrum of the dye. The WLC shows higher intensities below the ~550 nm. At the identical experimental condition, the solvent does not show any NLO effect.

At the pump wavelength of 772 nm, 2PA is possible provided that either (i) the photon density for degenerate-resonant 2PA is sufficiently high or (ii) the 2 step—non-degenerate 2PA takes place in which one photon of the pump and the other of SC below 630 nm is simultaneously present. In the present experiment, the generated SC is weak even at the pump wavelength, and thus, the 2PA transition has been shown for the generalised case at higher pump energies. Near the pump wavelength, the dye has enough single photon absorption resulting in dominant SA effect.

V. DISCUSSIONS

A. Saturable absorption

Figure 7 shows that the nonlinear transmission spectrum of the dye can be measured simultaneously for all wavelengths

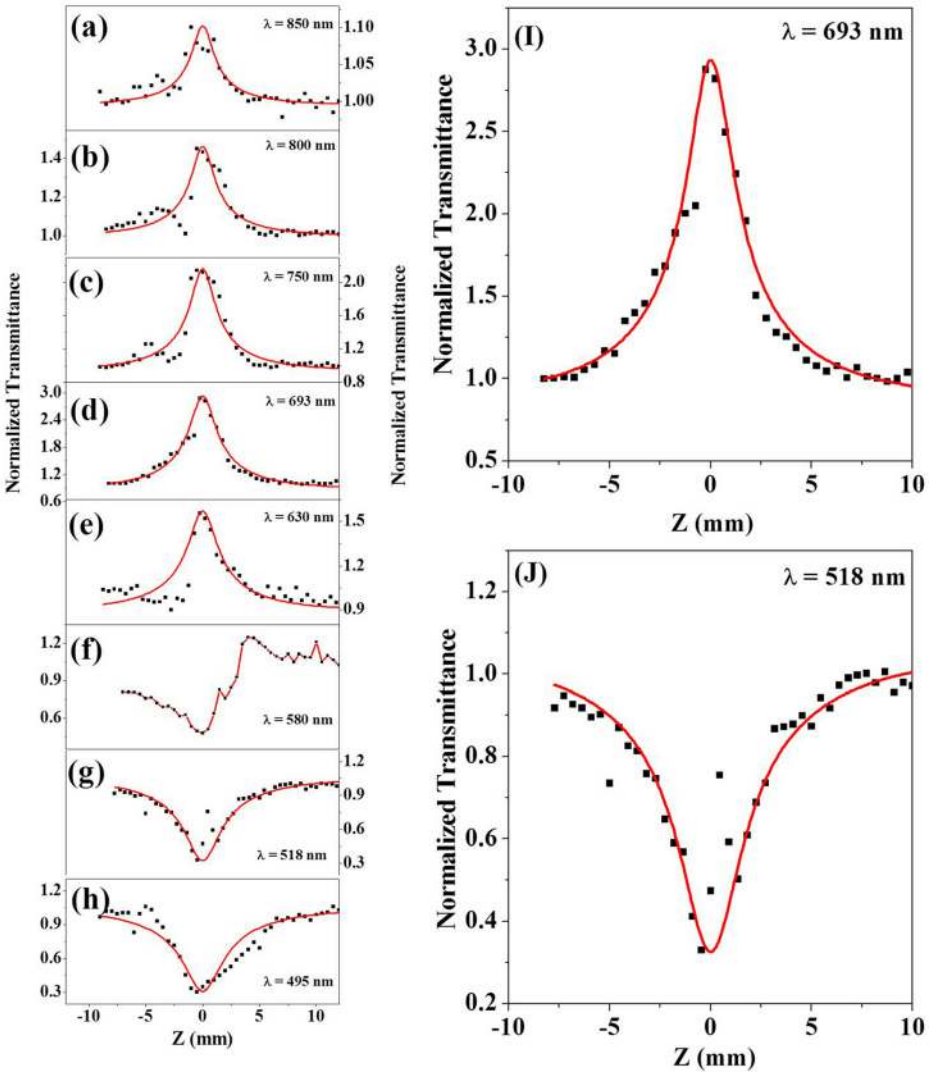

FIG. 7. OA Z-scan profiles of IR26 extracted from WL Z-scan. Symbols are experimental data and solid lines are guiding to the eye.

in the band with a single Z-scan measurement. Equally and importantly, note that RSA at nonresonant wavelengths (shorter than 580 nm) switches over to SA at resonant wavelengths (longer than 630 nm). SA is favoured when the excited state has a relatively longer lifetime, leaving the ground state depleted for further light absorption. However, the depletion process often requires several GW/cm^2 of intensity to achieve excitation rate higher than the relaxation rate. In the present case, the SA occurs at low intensity of ~130 MW/cm^2. Our results show that the SA can be achieved by an additional process as well. When there are multiple levels available, a broadband input pump (nondegenerate) can simultaneously excite many molecules, and thus, increasing the probability of emptying the ground state even at a lower intensity. The energy level diagram for multiple wavelength excitations for observed low saturation SA is shown in Figure 8.

The OA profile at 630 nm (Figure 7(e)) was fitted with Equation (2). Here, the input intensity 0.13×10^{13} W/m^2 considered for a range of wavelengths (610 nm–650 nm) is equal to the spectral width of the pump pulses. The obtained values of saturation intensity I_s, β and imaginary part of the susceptibility ($\chi^{(3)}_{Im}$) are 0.14×10^{12} (W/m^2), -7.6×10^{-9} (m/W), and -2.8×10^{-18} (m^2/V^2), respectively.

B. Reverse saturable absorption

1. Electronic nonlinearity

The RSA effect can be explained based on the combined effect of two photon absorption (2PA), excited state absorption (ESA), and thermo optical effects. The pulse width of the laser is 90 fs with a repetition rate of 82 MHz providing a delay time of 12.2 ns between the successive pulses. The excited state lifetime of IR26 is 22 ps.[38] It indicates that the successive pulses will not create any excited state absorption; only at high input intensities the same pulse can send it to higher states by either 2PA or ESA or by both the processes. For the wavelengths below 580 nm, the SA switches to RSA.

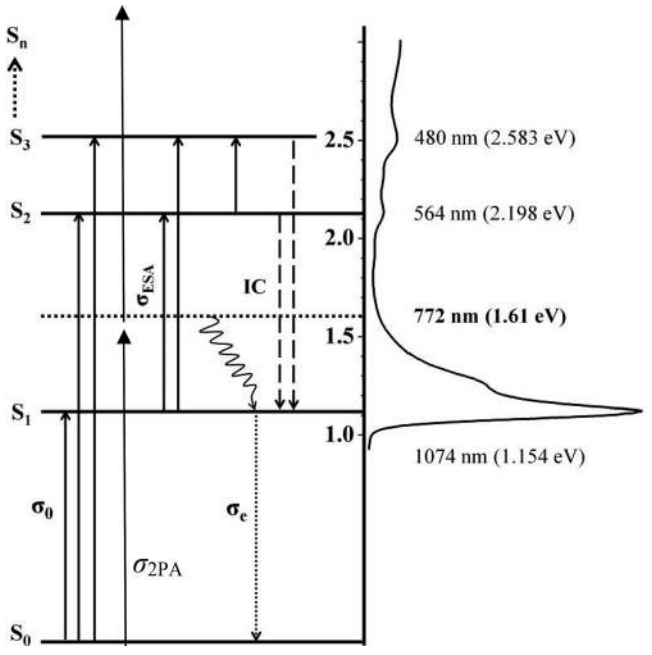

FIG. 8. Composite energy level diagram of IR26 to explain the possible mechanisms for SA and RSA. σ_0 is the ground state absorption cross-section, σ_e is the emission cross-section, σ_{ESA} is the excited state absorption cross-section, σ_{2PA} is the two photon absorption cross section and IC is the internal conversion. Excitation by the remaining pump wavelength (772 nm) helps in achieving broad band nonlinearity at low pump threshold. Dotted horizontal line indicates the vibrational level corresponding to 772 nm.

A composite energy level diagram of IR26 is given in Figure 8, to discuss the various factors that influence the low saturation SA and effect of RSA. Here S_n (n = 1,2,.) are singlet excited states, while S_o is the singlet ground state. σ's corresponds to the absorption and emission cross-sections, and IC depicts the internal conversion. The solvent relaxation time of 1,2-dichloroethane is the order of ps. Therefore, within this time the molecules return to S_1 nonradiatively and further relax back to S_0 radiatively as suggested by Kasha.[39]

It is to be noted that the remaining pump light of the fs laser (772 nm) will also carry molecules to the vibrational manifold of S_1. The effect of SA observed above 630 nm is due to bleaching of the ground state by excitation to the S_1 level. The RSA behaviour below 580 nm can be due to 2PA and excited state absorption from S_1 to higher energy levels. Combined effect of SA and RSA is observed from 580 nm to 630 nm. This is due to bleaching of ground state by excitation to S_2 level and excited state absorption from S_1 to higher energy levels.

2. Thermo-optical nonlinearity

Due to the high repetition rate of the laser, the thermo optical effect also plays a major contribution to the observed RSA effect.[40] In our experiments, the thermal effects are in the steady-state regime. The thermal rise (τ_{rise}) and relaxation (τ_{relax}) times for the solvent 1,2-dichloroethane at 518 nm have been calculated by using the following equations:

$$\tau_{rise} = \frac{\omega_0}{V_s}, \tag{4}$$

$$\tau_{relax} = \frac{\omega_0^2 \rho C_P}{4K}. \tag{5}$$

Here, V_s is the acoustic velocity, ρ, C_P and K are the solvent density, specific heat and thermal conductivity of the solvent, respectively, as given in Table II.

The estimated τ_{rise} and τ_{relax} are 7.5 ns and 0.28 ms, respectively. The repetition rate of the laser is much higher than the $1/\tau_{relax}$. In this case, the stationary lens will be formed. It can defocus the beam, or by self diffraction, the

TABLE II. Physical parameters of 1,2-dichloroethane.

Quantity	Values	References
Density (ρ)	1253 (kg/m^3)	41
Refractive index (n_0)	1.4448	
Specific heat (C_P)	1.30×10^3 (J/kg K)	42
Thermal conductivity (K)	0.1317 (W/m K)	43
Acoustic velocity (V_s)	1272 (m/s)	41

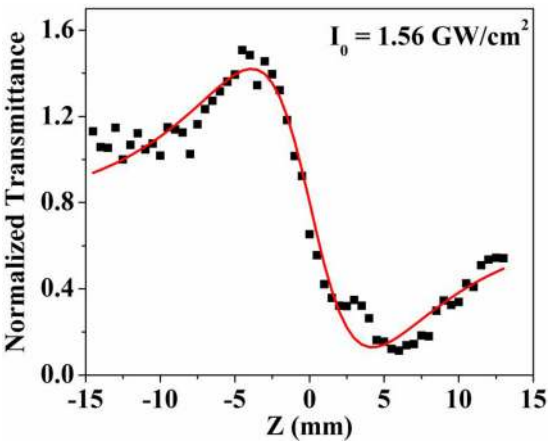

FIG. 9. CA Z-scan profile of IR 26 recorded at the fundamental wavelength (772 nm).

intensity at the detector position can be reduced leading to the effect of optical limiting. Closed aperture Z-scan profile of IR26 excited at fundamental wavelength alone is shown in Figure 9. The profile shows a peak followed by a valley indicating the self-defocusing nature of the sample. The RSA profile at 518 nm was fitted with Equation (3). The estimated β_{Eff} and $\chi^{(3)}_{\mathrm{Im}}$ are 2.7×10^{-8} (m/W) and 8.3×10^{-18} (m^2/V^2), respectively.

VI. CONCLUSIONS

nJ pulses of Ti: Sapphire oscillator have been used to generate SC from a PCF by pumping at 772 nm. The SC spectrum consists of wavelengths from 450 nm to 1700 nm. We have carried out the Z-scan experiments with broad band femtosecond white light pump. The broad band enables us to obtain the nonlinear parameters for *all* wavelengths in the visible band with a single Z-scan measurement, and the simultaneous excitations by photons of various wavelengths reduce the threshold for SA studies at a wavelength in the band. Further, we observed switching of RSA to SA behavior for longer wavelengths for the same input intensity. A comparison with the existing literature[10] confirms the RSA behavior at 532 nm under ps excitation.

ACKNOWLEDGMENTS

We thank Dr. Srini Krishnamurthy of SRI International for the fruitful discussions and critical reading of this manuscript. The financial support from the Defence Research and Development Organization (DRDO) and the Council of Scientific and Industrial Research (CSIR), New Delhi is gratefully acknowledged.

[1]*Quantum Electronics—Principles and Applications*, edited by P. F. Liao and P. L. Kelley (Academic Press, Inc., 1992).
[2]C. V. Bindhu, S. S. Harilal, V. P. N. Nampoori, and C. P. G. Vallabhan, J. Phys. D: Appl. Phys. **32**, 407 (1999).
[3]S. Luo, E. Zhang, Y. Su, T. Cheng, and C. Shi, Biomaterials **32**, 7127 (2011).
[4]M. Matsui, Y. Hashimoto, K. Funabiki, J.-Y. Jin, T. Yoshida, and H. Minoura, Synth. Met. **148**, 147 (2005).
[5]X. Yi, F. Yan, F. Wang, W. Qin, G. Wu, X. Yang, C. Shao, L. W. K. Chung, and J. Yuan, Med. Sci. Monit.: Int. Med. J. Exp. Clin. Res. **21**, 511 (2015).
[6]M. V. Bondar, A. D. Nadezhda, G. G. Dyadyusha, V. M. Zubarovskiĭ, A. I. Aleksandr, O. V. Przhonskaya, L. S. Yu, A. L. Smirnova, E. A. Tikhonov, and I. T. Alexei, Sov. J. Quantum Electron. **14**, 317 (1984).
[7]Q. Bellier, N. S. Makarov, P.-A. Bouit, S. Rigaut, K. Kamada, P. Feneyrou, G. Berginc, O. Maury, J. W. Perry, and C. Andraud, Phys. Chem. Chem. Phys. **14**, 15299 (2012).
[8]A. Seilmeier, B. Kopainsky, and W. Kaiser, Appl. Phys. **22**, 355 (1980).
[9]C. Continuum Model YG601, Santa Clara, CA.
[10]B. S. Kalanoor and P. B. Bisht, Opt. Commun. **283**, 4059 (2010).
[11]S. A. Ali, P. B. Bisht, B. S. Kalanoor, A. Patra, and S. Kasiviswanathan, J. Opt. Soc. Am. B **30**, 2226 (2013).
[12]J. Wang, Y. Hernandez, M. Lotya, J. N. Coleman, and W. J. Blau, Adv. Mater. **21**, 2430 (2009).
[13]Y. Jiang, L. Miao, G. Jiang, Y. Chen, X. Qi, X.-F. Jiang, H. Zhang, and S. Wen, Sci. Rep. **5**, 16372 (2015).
[14]B. Anand, R. Podila, P. Ayala, L. Oliveira, R. Philip, S. S. Sankara Sai, A. A. Zakhidov, and A. M. Rao, Nanoscale **5**, 7271 (2013).
[15]N. K. M. N. Srinivas, S. V. Rao, and D. N. Rao, J. Opt. Soc. Am. B **20**, 2470 (2003).
[16]R. S. S. Kumar, S. V. Rao, L. Giribabu, and D. N. Rao, Chem. Phys. Lett. **447**, 274 (2007).
[17]Z.-B. Liu, Y.-L. Liu, B. Zhang, W.-Y. Zhou, J.-G. Tian, W.-P. Zang, and C.-P. Zhang, J. Opt. Soc. Am. B **24**, 1101 (2007).
[18]D. Sharma, P. Gaur, B. P. Malik, N. Singh, and A. Gaur, Opt. Photonics J. **2**, 98 (2012).
[19]S. Perumbilavil, P. Sankar, T. Priya Rose, and R. Philip, Appl. Phys. Lett. **107**, 051104 (2015).
[20]M. Balu, J. Hales, D. J. Hagan, and E. W. V. Stryland, Opt. Express **12**, 3820 (2004).
[21]L. A. Padilha, G. Nootz, M. Balu, D. J. Hagan, E. W. Van Stryland, S. Zheng, S. Barlow, and S. R. Marder, in *Nonlinear Optical Characterization of Organic Molecules Using a White-Light Continuum Z-Scan, San Jose, California, 2007* (Optical Society of America, 2007), p. FMG2.
[22]L. D. Boni, A. A. Andrade, L. Misoguti, C. R. Mendonça, and S. C. Zilio, Opt. Express **12**, 3921 (2004).
[23]G. S. He, T.-C. Lin, P. N. Prasad, R. Kannan, R. A. Vaia, and L.-S. Tan, Opt. Express **10**, 566 (2002).
[24]R. R. Alfano and S. L. Shapiro, Phys. Rev. Lett. **24**, 592 (1970).
[25]A. Nautiyal and P. B. Bisht, Opt. Commun. **278**, 175 (2007).
[26]P. Vasa, J. A. Dharmadhikari, A. K. Dharmadhikari, R. Sharma, M. Singh, and D. Mathur, Phys. Rev. A **89**, 043834 (2014).
[27]J. Liu, H. Schroeder, S. L. Chin, R. Li, and Z. Xu, Opt. Express **13**, 10248 (2005).
[28]P. B. Corkum, C. Rolland, and T. Srinivasan-Rao, Phys. Rev. Lett. **57**, 2268 (1986).
[29]J. K. Ranka, R. S. Windeler, and A. J. Stentz, Opt. Lett. **25**, 25 (2000).
[30]R. V. J. Raja, A. Husakou, J. Hermann, and K. Porsezian, J. Opt. Soc. Am. B **27**, 1763 (2010).
[31]A. Bozolan, C. J. S. de Matos, C. M. B. Cordeiro, E. M. dos Santos, and J. Travers, Opt. Express **16**, 9671 (2008).
[32]I. Z. Kozma, P. Baum, U. Schmidhammer, S. Lochbrunner, and E. Riedle, Rev. Sci. Instrum. **75**, 2323 (2004).
[33]M. Sheik-Bahae, A. A. Said, T. H. Wei, D. J. Hagan, and E. W. V. Stryland, IEEE J. Quantum Electron. **26**, 760 (1990).
[34]R. A. Ganeev, R. I. Tugushev, and T. Usmanov, Appl. Phys. B **94**, 647 (2009).
[35]*Progress on Tunable Lasers for Ultrafast Processes and Applications*, edited by P. B. Bisht (Research Publishing, Chennai/Singapore, 2006).
[36]S. Coen, A. H. L. Chau, R. Leonhardt, J. D. Harvey, J. C. Knight, W. J. Wadsworth, and P. S. J. Russell, Opt. Lett. **26**, 1356 (2001).
[37]C. Lin and R. H. Stolen, Appl. Phys. Lett. **28**, 216 (1976).
[38]B. Kopainsky, P. Qiu, W. Kaiser, B. Sens, and K. H. Drexhage, Appl. Phys. B **29**, 15 (1982).
[39]M. Kasha, Discuss. Faraday Soc. **9**, 14 (1950).
[40]F. Z. Henari and P. S. Patil, Opt. Photonics J. **4**, 182 (2014).
[41]H. Kumar and D. Kumar, Int. J. Thermodyn. **16**, 9 (2013).
[42]M. J. Weber, *Handbook of Optical Materials* (CRC Ppress, Lawrence Berkeley National Laboratory, University of California, Berkeley, California, 2002).
[43]L. Qun-Fang, L. Rui-Sen, N. Dan-Yan, and H. Yu-Chun, J. Chem. Eng. Data **42**, 971 (1997).